Lasers in Surgery and Medicine 19:471–479 (1996)

Anisotropy of Radiance in Tissue Phantoms and Dunning R3327 Rat Tumors: Radiance Measurements With Flat Cleaved Fiber Probes

Åse M. Ballangrud, PhD, Peter J. Wilson, MSc, Kevin Brown, Gerald G. Miller, PhD, Ronald B. Moore, MD, PhD, Malcolm S. McPhee, MD, MSc, and John Tulip, PhD

University of Alberta, Department of Electrical Engineering, Edmonton, AB, T6G 2G7 (Å.M.B., P.J.W., J.T); and Cross Cancer Institute, Department of Surgery, Edmonton, AB, T6G 1Z2 (K.B., G.G.M., R.B.M., M.S.McP.)

Background and Objective: **The goal of this study is to determine if flat cleaved fiber probes are appropriate for interstitial measurements of radiance in tissue. Flat cleaved probes have the advantage of high responsivity, and they are easy to insert into tissue. Owing to the non-isotropic response of flat cleaved probes, a calibration function is required, taking the anisotropy in the radiance in tissue into account.**

Study Design, Materials and Methods: **The method used to determine this function consists of radiance measurements in tissue, performed with a flat cleaved fiber probe mounted on a stereotactic stage for insertion into the tissue from different directions. Interstitial irradiation at 630 nm was delivered by a spherical source.**

Results: **We found that the degree of anisotropy in the radiance decreases with increasing distance from the interstitially implanted source in two different tissue phantoms and in the Dunning R3327-AT and R3327-H rat tumor models.**

Conclusion: **A position-dependent calibration function is required for interstitially implanted flat cleaved fiber probes. An anisotropy function is presented, which modifies the measurements of radiance with a flat cleaved probe, to account for the change in anisotropy in the radiance. The anisotropy functions for the two tumor models differ substantially.**

Key words: dosimetry, interstitial light detection, light distribution, non-isotropic probes, photodynamic therapy, solid tumors

INTRODUCTION

Interactions between light and tissue are determined by scattering and absorption [1]. The optical coefficients of solid tumors can be found indirectly by using a mathematical model of light propagation in conjunction with experimental data of light radiance (flux of optical energy in a particular direction per unit solid angle and per unit area normal to the direction of propagation) in the tissue, performed with interstitially implanted fiber probes. A comparison between direct and indirect methods for measurements of the optical coefficients in tissue has been published by Wilson et al. [2]. Several mathematical models have been compared, and their ability to quantitatively describe radiance in tissue and to determine the optical properties of tissue, and tissue

Accepted for publication June 30, 1995.

Address reprint requests to Åse M. Ballangrud, Cross Cancer Institute, Department of Surgery, 11560 University Ave., Edmonton, Alberta T6G 1Z2, Canada.

phantoms, has been studied [3–8]. Measurements of optical coefficients have been performed with interstitial irradiation in solid tumors, and specifically in prostate tissue and tumor models [3,9–11], by fitting different mathematical models to data of measured radiance. Light scattering in tissue is known to be mainly forward-directed. The scattering function has been measured for some tissues [12], but, in general, the lack of knowledge on the scattering function complicates modeling of light propagation in tissues. The strong forward scattering will cause an anisotropic radiance, which will become less anisotropic as the photons undergo multiple scattering. Some degree of anisotropy will however persist after many scattering events because of absorption. In a previous publication [13], we showed that the degree of anisotropy in the radiance changes in tissue phantoms over a distance relevant to PDT.

The accuracy of the optical coefficients found indirectly from radiance measurements depends on how well the mathematical model describes light propagation in tissue. Some of the mathematical models used for modeling of light propagation in tissue and tissue phantoms are based on diffusion theory [14,15], others on analytical solutions of the transport equation (Boltzman equation) for specific geometries [3,6], or numerical simulations as Monte Carlo modeling [4,7] and discrete ordinates methods [5]. Analytical solutions to the Boltzman equation for the space irradiance (radiance integrated over the solid angle) of a point source in an infinite, homogenous medium have been developed by Grosjean [16] and Weinberg and Wigner [17]. The Grosjean and Weinberg-Wigner models calculate the space irradiance, and information on the angular dependency of the radiance is not included in these models. The most general mathematical technique for modeling light propagation in tissue is the Monte Carlo method, which allows the inclusion of complex boundary effects and arbitrary inhomogenities within the tissue.

The cell killing ability of photodynamic therapy depends on the space irradiance at each point in the tumor, independent of the direction of light propagation. Measurements of local light intensity in tissue can be performed with spherical probes with isotropic response, or with flat cleaved (flat ended) fibers having non-isotropic response. An isotropic probe would provide data of the space irradiance. The responsivity of the isotropic probes increases with increasing fiber core diameter [6]; however, larger probes are difficult to insert into the tissue. Flat cleaved probes have the advantage that they are easy to use interstitially in tissue when mounted into steel needles. They are much less fragile than the isotropic probes. When measurements are made along a line from the source, our experience is that the signal level is larger for a flat cleaved probe than for an isotropic probe with equal fiber core diameter. The disadvantage of the flat cleaved probes is that the signal level depends on the orientation of the probe relative to the source due to the anisotropy of the radiance in tissue. A calibration has to be performed due to the non-isotropic response of this probe. Inaccuracies will result if the radiance measured with a flat cleaved fiber probe is compared directly with the Grosjean- and the Weinberg-Wigner-modeled space irradiance. In previous work [3], we assumed this calibration factor to be independent of position, but we have now found that it is dependent on distance from the source. The changes in anisotropy of the radiance are significant over a distance relevant to PDT. In the following, we report on this calibration function, which we call an anisotropy function, in two different tissue phantoms and in the anaplastic Dunning R3327-AT and the well differentiated R3327-H rat tumor models.

Measurements of angular variations in the radiance will give additional information on light propagation in tissue, and this information is useful in construction of a model for light distribution. Differences in tissue structure may give different radiance. The mathematical model must be capable of taking changes in radiance over distance into account, so that the optical coefficients can be determined. This is important for light dosimetry in PDT.

The radiance in a tissue phantom is measured as described in a previous publication [13]. A flat cleaved fiber is mounted on a rotational stage and the radiance from several directions was measured at different distances from the source fiber. Measurements of radiance in tissue are more complicated. We performed measurements by using a stereotactic stage where the probe fiber was inserted into the tissue from different angles. Alternatively, the anisotropy function can be found by comparing measurements of the radiance performed with a flat cleaved fiber probe and measurements of the space irradiance with a spherical probe. Quantitative measurement of the anisotropy function is complicated by the fact that the responsivities of both fiber

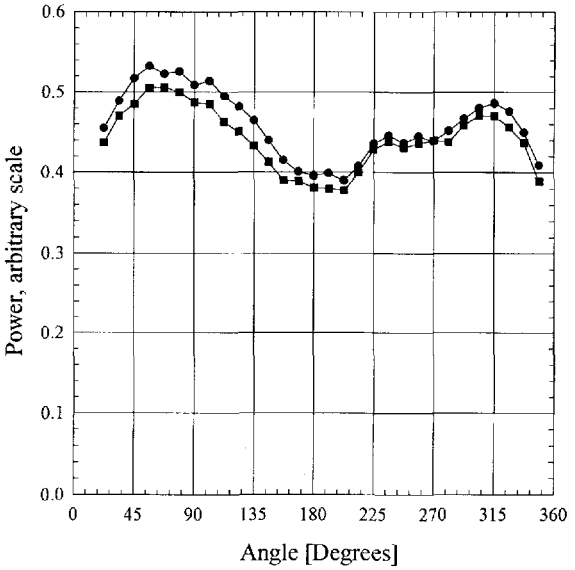

Fig. 1. Irradiation pattern for the spherical source. The angular distribution of light from the tip was measured by moving a detector head along a circle with diameter 30 cm around the fiber tip. Measurements were performed in two perpendicular planes by rotating the tip 90°.

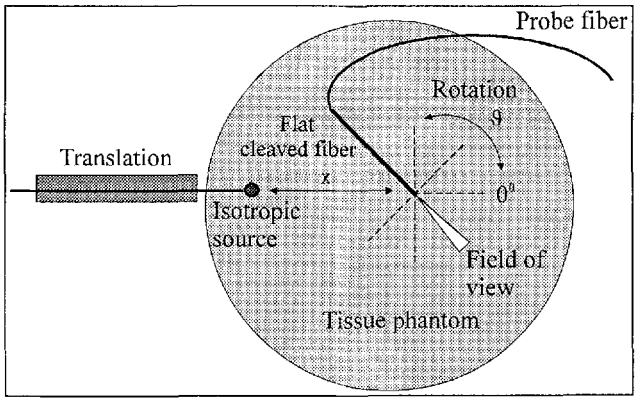

Fig. 2. Illustration of the set-up for measurements of angular dependency of the radiance in tissue phantoms. The detector probe was mounted on a rotational stage so that the probe could be rotated (ϑ), keeping the tip at the center point. The source fiber was mounted on a translation stage, and the distance (x) between the source and the probe could be changed. In this way, the radiance from different directions could be measured at different distances from the source. Measurements were performed at 2 mm intervals, out to 16 mm from the source.

probes have to be known. The responsivity of the spherical detector is not easily determined.

MATERIALS AND METHODS

Set-Up

An argon-ion laser (Spectra-Physics, Mountain View, CA) pumped dye laser (Coherent, Santa Clara, CA) irradiating at 630 nm was used for all measurements of radiance. The laser light was coupled to a 400 μm core optical fiber with a spherical diffusing tip at the distal end. This isotropic irradiator was used for light delivery in the tissue phantoms and in the tumor models. The diameter of the spherical tip was 3 mm. The power output at the distal end was set to 200 mW. The irradiation pattern of the spherical source fiber varied about ± 10% about the mean value (Figure 1).

The detector fiber was a flat cleaved optical fiber (flat ended fiber) with core diameter 400 μm. The outer jacket was stripped off the fiber and the fiber was mounted into a steel needle, with a beveled tip to ease penetration into tissue. The numerical aperture of the flat cleaved fiber probe was 0.2 in air, corresponding to an acceptance angle (half angle) of 11.5°. Local light intensity was detected with a flat cleaved probe and quantified with a silicon photodiode in an integrating sphere (United Detector Technology, Hawthorne, CA).

The angular dependency of the radiance in tissue phantoms was measured with the detector probe mounted on a rotational stage so that the probe could be rotated, always keeping the tip at the center point. The source fiber was mounted on a translation stage and measurements were performed at different distances from the source. This is illustrated in Figure 2. The tissue phantom container was 7 cm deep and 25 cm in diameter and measurements were performed in such a way to minimize boundary effects.

Measurements of radiance in the tumor tissue were performed on excised tumors, which had been stored frozen. Experiments were performed on three R3327-H tumors and on four R3327-AT tumors. The angular dependency of the radiance was measured as illustrated in Figure 3, where the spherical source fiber was inserted into the tumor and held in the same position during the measurements. Only the probe fiber was moved. The flat cleaved probe was mounted on a stereotactic stage where the probe could be inserted from different angles with an angular accuracy of ± 1° and with a translation accuracy of ± 0.05 mm. Measurements were performed at 20 mm, 16 mm, 12 mm, 8 mm, 4 mm, and 2 mm, approaching the source to avoid perforation artifacts. Two of the R3327-AT tumors were large enough to facilitate measurements up to 20 mm, the third and

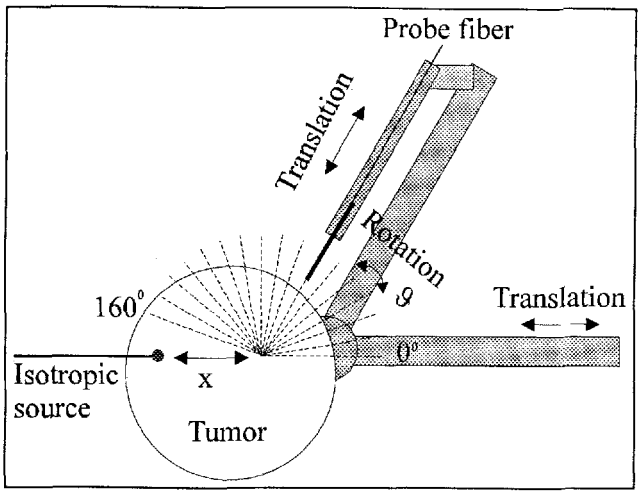

Fig. 3. Illustration of the set-up for measurements of angular dependency of the radiance in Dunning R3327-AT and R3327-H tumors, excised from rats. A flat cleaved probe fiber was mounted on the stereotactic stage and inserted into the tumor at different angles (ϑ). The rotational stage was mounted on a translation stage and could be moved (x) so that the probe fiber, and hence the center point for detection, could be moved toward the source. The broken lines show the insertion tracks for the probe fiber.

fourth tumors provided data to 16 mm and 12 mm, due to their smaller size. For the R3327-H tumors, measurements were performed in one tumor to 20 mm, for the second to 12 mm, and for the third up to 8 mm.

Tissue Phantoms

Two tissue phantoms with slightly different absorption and scattering coefficients at 630 nm were made from Intralipid (Kabi Pharmacia Baie d'Urfe, Quebec, Canada, 10% Intralipid, containing 10 g purified soybean oil, 1.2 g purified egg phospholipids, and 2.2 g glycerin anhydrous in 100 ml injectable solution), Methylene Blue (Fisher Scientific, Fair Lawn, NJ) and distilled water. At 630 nm, Intralipid, like tissue, is highly preferentially forward scattering, and it has a weak absorption. The phantoms were made so that the optical coefficients at 630 nm were in the range of published data on optical coefficients for the Dunning tumor models [3,9]. Published data on absorption and scattering coefficients of Intralipid [18,19] were used to design the phantoms. The phantom with highest absorption and scattering coefficients (phantom 1) consists by volume of 3.8% Intralipid, 0.4% Methylene Blue (1 μg/μl dissolved in distilled water), and 95.8% distilled water. Phantom 2 consists by volume of 1.73% Intralipid, 0.18% Methylene Blue (1 μg/μl dissolved in distilled water), and 98.09% distilled water. The absorption and scattering coefficients at 630 nm were measured with a spectrophotometer (Beckman DU7400, Fullerton, CA), using different dilutions of the phantoms in water to ensure linearity of the measured absorbance with increasing concentration. At 630 nm, the measured absorption and scattering coefficients of phantom 1 were 0.96 ± 0.09 cm^{-1} and 15.64 ± 0.93 cm^{-1}, respectively. For phantom 2, the coefficients were 0.43 ± 0.04 cm^{-1} and 6.97 ± 0.29 cm^{-1}, respectively.

Dunning R3327 Tumor Models

Dunning tumors are considered to represent reasonable models of human prostate cancer [20,21]. The R3327-AT subline exhibits anaplastic histology, has a doubling time of 2–3 days, and is relatively poorly perfused. The R3327-H tumor exhibits well-differentiated histology, has a doubling time of 10–15 days, and is well perfused. Both tumors were maintained by serial transplantation of tumor fragments in the flanks of male Fisher × Copenhagen rat F_1 hybrids.

ANISOTROPY FUNCTION

In comparing the results of the model to the experimental data we must deal with the fact that several models give the position-dependent space irradiance, Φ(x), while the experimental data are the radiance measured by the flat cleaved fiber with non-isotropic response. For a flat cleaved fiber, the measured power relates to the radiance φ(x,Ω) by the equation

$$W_f(x,\Omega) = RA\Omega_a\varphi(x,\Omega), \quad (1)$$

where $W_f(x,\Omega)$ is the power measured by the detector, x is the distance between the source and the probe fiber, Ω is the orientation solid angle of the probe relative to the source, R is the responsivity of the flat cleaved fiber probe and the detector, A is the cross-sectional area of the fiber, Ω_a is the acceptance solid angle of the fiber, and φ(x,Ω) is radiance, which depends both on position and angle. The radiance is related to the space irradiance according to the equation

$$\Phi(x) = \int_{4\pi} \varphi(x,\Omega)d\Omega. \quad (2)$$

The position-dependent space irradiance is the integral of the angle and position-dependent radi-

ance over 4π solid angle. Should the radiance $\varphi(x,\Omega)$ be isotropic, that is independent of angle, the equation can be reduced to

$$\Phi(x) = 4\pi\varphi(x). \tag{3}$$

It is well known that light is mainly forward-scattered in tissue [12]. In both phantoms and tumors our measurements indicate that the degree of anisotropy in the radiance changes from strongly anisotropic close to the source, to less anisotropic further away from the source. To include the effects of a position-dependent anisotropy in the radiance in our measurements with a flat cleaved probe, we defined the anisotropy function $C_{fc}(x,\Omega)$, a calibration function due to the non-isotropic response of the flat cleaved fiber probe. This anisotropy function depends on both position and angle and is defined to satisfy the equation

$$\varphi(x,\Omega) = \bar{\varphi}(x)C_{fc}(x,\Omega), \tag{4}$$

where the mean radiance $\bar{\varphi}(x)$ is defined by

$$\bar{\varphi}(x) = \frac{\int \varphi(x,\Omega)d\Omega}{\int d\Omega} = \frac{1}{4\pi}\int_{4\pi}\varphi(x,\Omega)d\Omega. \tag{5}$$

The anisotropy function is then given by

$$C_{fc}(x,\Omega) = \frac{\varphi(x,\Omega)}{\bar{\varphi}(x)} = \frac{4\pi\varphi(x,\Omega)}{\int_{4\pi}\varphi(x,\Omega)d\Omega} = \frac{4\pi W_f(x,\Omega)}{\int_{4\pi}W_f(x,\Omega)d\Omega}. \tag{6}$$

The anisotropy function equals unity for isotropic radiance. From equation (6), we can determine $C_{fc}(x,\Omega)$ from the measured data $W_f(x,\Omega)$, which is proportional to the radiance $\varphi(x,\Omega)$. From equations (1), (2), and (6), the relation between the radiance in the tumor tissue, measured with a flat cleaved probe, and the modeled space irradiance $\Phi(x)$ is then expressed as

$$W_f(x,\Omega) = \frac{RA\Omega_a}{4\pi}C_{fc}(x,\Omega)\Phi(x). \tag{7}$$

The integral in the denominator of equation (6) is derived from the measured radiance data. Owing to the nature of the experiment, it was impossible to obtain experimental data of the radiance for the entire 4π range. We make the assumption that the radiance anisotropy depends only on the azimuth angle ϑ. This assumption holds only for homogenous media. In an inhomogenous medium, like tissue, the radiance will also depend on local optical coefficients and will vary with polar angle. The element of solid angle $d\Omega$ can be written as $\sin(\vartheta)d\vartheta d\xi$ in terms of ϑ and the polar angle ξ, giving

$$\int_{4\pi}W_f(x,\Omega)d\Omega = \int_{\xi=0}^{2\pi}\int_{\vartheta=0}^{\pi}W_f(x,\vartheta)\sin(\vartheta)d\vartheta d\xi = 2\pi\int_{\vartheta=0}^{\pi}W_f(x,\vartheta)\sin(\vartheta)d\vartheta. \tag{8}$$

A numerical fit to the data was employed to extrapolate into the region where measurements could not be performed. The function used to fit to the data was based on the radiance for isotropic scattering and slab geometry [22]. The fit had the form

$$W_f(x,\vartheta) = \frac{B(x)}{1 - A(x)\cos(\vartheta)}, \tag{9}$$

where $A(x)$ and $B(x)$ are position-dependent factors which are determined from the experimental data by least squares optimization. Equation (9) fits the data with a correlation coefficient in the range 0.97–0.99. We use the convention that the probe fiber oriented toward the source is 0°, and the reverse orientation is 180°. For convenience, the fit in equation (9) was used over the entire circle, allowing evaluation of the integral in equation (8) analytically, giving

$$\int_{4\pi}W_f(x,\Omega)d\Omega = \frac{2\pi B(x)}{A(x)}\ln\left(\frac{1 + A(x)}{1 - A(x)}\right). \tag{10}$$

The anisotropy function $C_{fc}(x,\vartheta)$ is then given from equation (6) and (10) by

$$C_{fc}(x,\vartheta) = \frac{2W_f(x,\vartheta)}{\frac{B(x)}{A(x)}\ln\left(\frac{1 + A(x)}{1 - A(x)}\right)}. \tag{11}$$

We prefer to perform measurements of radiance in tumor tissue with the flat cleaved fiber probe viewing the source fiber, which corresponds to radiance measurements in the 0° direction,

$W_f(x,0°)$. Therefore, in the following the anisotropy function for the flat cleaved probe is found for a fiber oriented towards the source, $C_{fc}(x,0°)$.

RESULTS

Radiance in Tissue Phantoms

Measured radiance in tissue phantoms 1 and 2 is shown in Figure 4a and 4b, respectively. The data are normalized to unity in the forward direction (0° orientation of the probe fiber). Measurements of the radiance were performed every 2 mm, between 2 mm and 16 mm.

The anisotropy function $C_{fc}(x,0°)$ was determined from equation (11). A curve fit was performed to calculate the radiance in the angular range, where measurements could not be performed. The anisotropy functions for tissue phantom 1 and 2, are shown Figure 5. Phantom 2 has lower absorption and scattering coefficients, and therefore a longer mean free path than phantom 1. This results in a more anisotropic radiance in phantom 2 than in phantom 1 at a given physical distance from the source.

Radiance in Dunning R3327-AT and R3327-H Tumors

The angular dependency of the radiance in tumor tissue was measured as described above. Radiance was measured in the range 0–160° at different distances from the spherical source in the tumor models. Radiance in the Dunning R3327-AT and Dunning R3327-H tumors is shown in Figure 6a and 6b, respectively. The data are normalized to unity in the forward direction.

In the tumor models, the anisotropy function was determined from a curve fit to extend the data through the entire 360°, and by application of equation (11). The anisotropy functions for the radiance in Dunning R3327-AT and R3327-H tumor, are shown Figure 7. Four different R3327-AT tumors and three R3327-H tumors were used in the experiment. There is a substantial difference in the anisotropy function for the two tumor models.

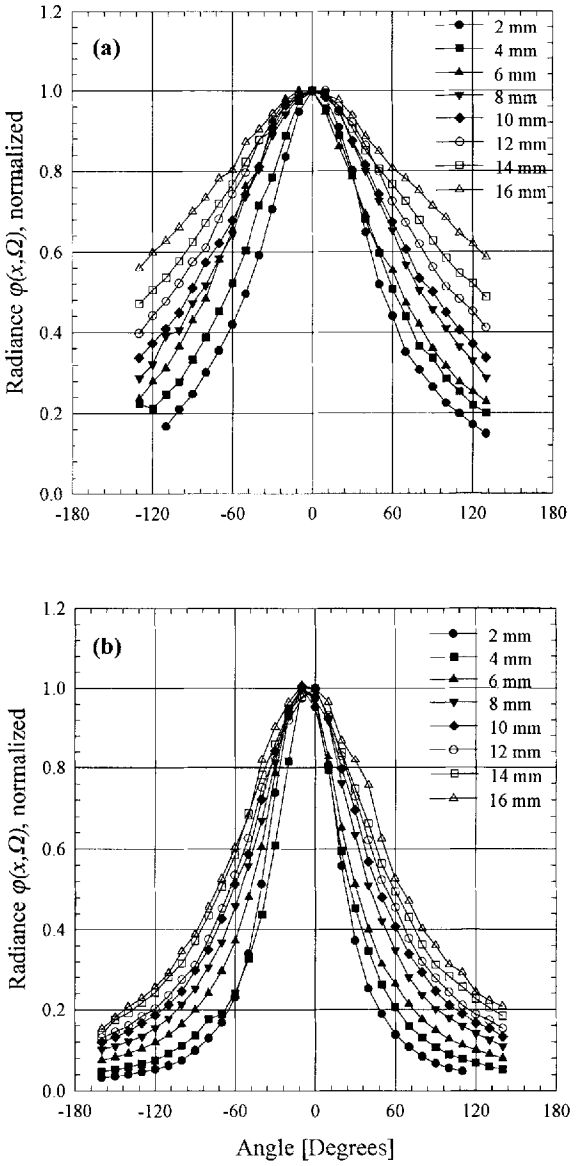

Fig. 4. Radiance as a function of angle in tissue phantom 1 (**a**) and phantom 2 (**b**). Phantom 1 has an absorption coefficient of 0.96 ± 0.09 cm^{-1}, and a scattering coefficient of 15.64 ± 0.93 cm^{-1}. For phantom 2, the coefficients are 0.43 ± 0.04 cm^{-1} and 6.97 ± 0.29 cm^{-1}, respectively. The lower absorption and scattering coefficients in phantom 2 causes a higher degree of anisotropy of the radiance close to the source. The data are normalized to unity in the forward direction.

DISCUSSION

This study shows that the anisotropy of the radiance in the Dunning tumor models changes over distances relevant to PDT. This is important for the use of flat cleaved fiber probes for interstitial measurements of radiance in tissue. The angular variation in the radiance from one tumor model to the other is substantial, and the anisotropy function must be known for the specific tissue sample so that the measured radiance can be corrected for the non-isotropic response of the fiber probe. The change in anisotropy in the radiance is also important for development of a mathematical model describing light propagation in tissue.

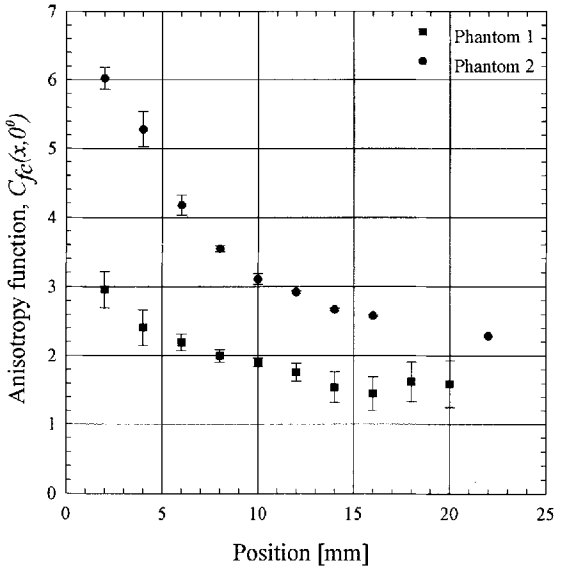

Fig. 5. Anisotropy function for phantoms 1 and 2. Four independent measurements were performed for phantom 1, and two for phantom 2. The standard deviation in the anisotropy function varies from the average value in the range 4–21% for phantom 1, and in the range 0.6–5% for phantom 2. Both the absorption coefficient and the scattering coefficient at 630 nm are higher in phantom 1 than in phantom 2. This causes a substantial difference in the anisotropy factor for the two phantoms. The photons undergo multiple scattering and the radiance becomes more isotropic.

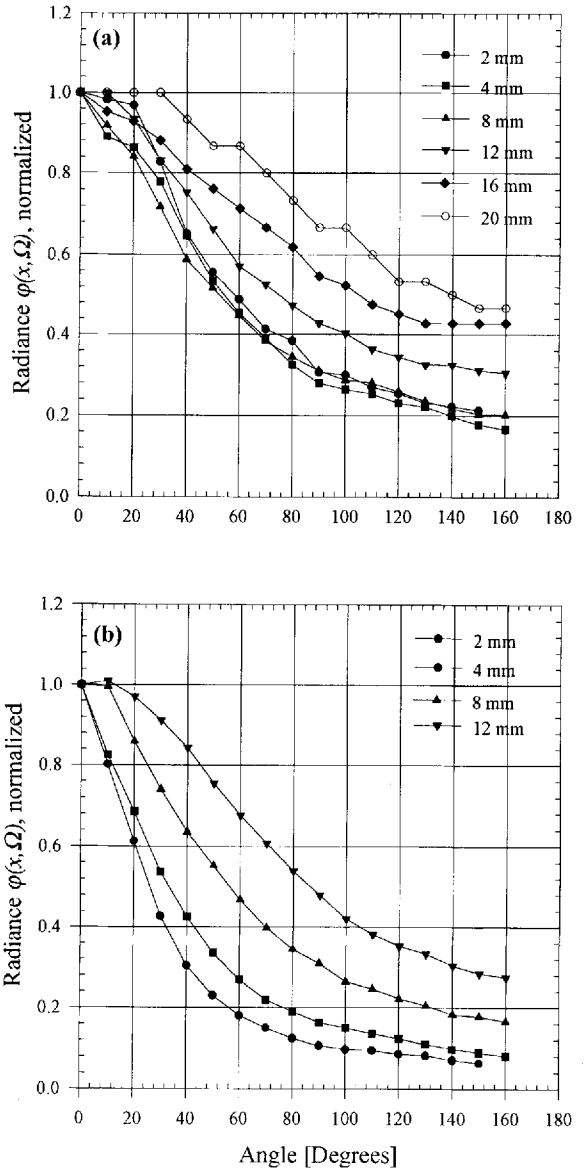

Fig. 6. Radiance as a function of angle in Dunning R3327-AT (**a**) and R3327-H (**b**) rat tumor models. The radiance is more anisotropic close to the source fiber than further away from the source. The tumor diameter was 28 mm for the anaplastic R3327-AT tumor. The diameter of the well-differentiated R3327-H tumor was 22 mm, and measurements could only be performed to 12 mm. The data are normalized to unity in the forward direction.

The anisotropy function is quite similar within the same tumor model, but there is a substantial difference in the anisotropy function between the two models. The anaplastic R3327-AT tumor has a lower degree of anisotropy close to the source fiber than the well-differentiated R3327-H tumor. The anisotropy functions for the R3327-H and R3327-AT tumors indicate that the absorption and scattering coefficients are lower in the R3327-H tumors than in the R3327-AT tumors, or that the scattering phase function for the two tumor models is different. The anisotropy function is determined with a standard deviation in the range 10–21% for the R3327-H tumors and 4–17% for the R3327-AT tumors, depending on position. The standard deviations for these two tumor models include an uncertainty due to the positioning of the probe and also to histological differences among the tumors.

The use of flat cleaved fiber probes in interstitial measurements of radiance in tissue has the advantage of high responsivity compared to small, spherical probes with isotropic response. Flat cleaved probes are also easier to insert into tissue than spherical probes. Flat cleaved fiber probes are only practical for radiance measurements in tissue if an anisotropy function can be determined as described in this study for the specific tissue. The difference in anisotropy function for the two tumor models reflects a difference in the tissue structure. It may also be possible to determine an anisotropy function based on information on the tissue from biopsy slides. If the an-

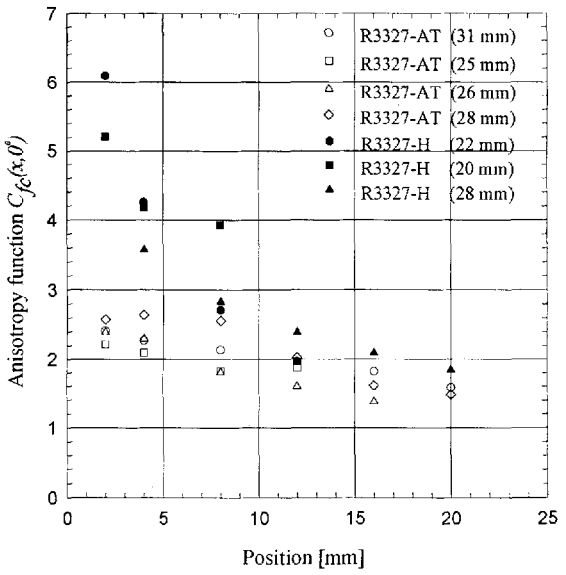

Fig. 7. Anisotropy function for excised Dunning R3327-AT and R3327-H tumors. Measurements were performed in three R3327-H tumors, and in four R3327-AT tumors. The diameters of the tumors are given in brackets in the legend. The radiance in the smaller tumors could not be measured out to 20 mm. The difference in the anisotropy function for the two tumor models is substantial, and reflects differences in the absorption and scattering coefficients, and possibly also in the scattering phase function, in the two tumor models. The standard deviation from the average value of the anisotropy function within the tumor models are in the range 10–21% for the R3327-H tumor and in the range 4–17% for the R3327-AT tumors.

isotropy function can be determined, the optical coefficients of the tissue can be found by comparing measured radiance with a mathematical model. The accuracy of the optical coefficients then depends on how well the model predicts the light propagation in tissue. The model must be able to predict the changes in radiance over distance, depending on the scattering phase function and the absorption and scattering coefficients of the tissue.

The diameters of the tumors used in this experiment were in the range 20–31 mm. The spherical source was implanted interstitially into the tumor about 5 mm from the tumor edge. The probe fiber was also about 5 mm from the edge for the measurements furthest away from the source. This may cause boundary artifacts, but the difference in tumor size does not seem to influence the anisotropy function in Figure 7. The measurements on the tumor models compare well with the measurements in the phantoms, where boundary artifacts were negligible.

The excised tumors were stored frozen until they were used in the experiments. Freezing disrupts cellular and subcellular membranes, which might perturb the light scattering properties. Also blood supply is absent. Measurements of radiance should be performed *in vivo* to determine the anisotropy function in living tumors.

Phantom 1 has higher absorption and scattering coefficients at 630 nm than phantom 2. The radiance for phantom 1 has a lower degree of anisotropy close to the source than phantom 2. This is reasonable, due to the lower scattering and absorption coefficient of phantom 2. The scattering centers in both phantoms are particles in the Intralipid. Therefore, the scattering phase function is the same in the two phantoms. The particle size in Intralipid is less than 1 μm [12,19]. The scattering phase function in the phantoms will likely always differ from the scattering phase function in tissue. This must be considered when tissue phantoms containing Intralipid are used for light propagation experiments.

The mathematical models which are analytical solutions to the Boltzman equation (transport theory) are all assuming an isotropic scattering phase function. These models are modified to take forward scattering in tissue into account, by replacing the scattering coefficient with a reduced scattering coefficient. The Grosjean and Weinberg-Wigner models do not include information on the angular dependency of the radiance and cannot be used to compare the measured radiance with a mathematical model. Approximate numerical solutions like a Monte Carlo simulation or a discrete ordinates methods where the angular dependency is discretized, allow calculation of the angular dependency of the radiance. These models should be compared with experimental data.

CONCLUSION

The anisotropy of the radiance changes over distances relevant to PDT, and this must be taken into account when flat cleaved probes with non-isotropic response are used for interstitial detection of radiance in tissue. The anisotropy function differs substantially between the anaplastic R3327-AT tumor and the well-differentiated R3327-H tumor model. The variation within each tumor model is small, and it seems possible to determine an anisotropy function for each of the tumor models.

ACKNOWLEDGMENTS

We would like to thank the National Cancer Institute of Canada, Terry Fox Program Project, the Alberta Heritage Foundation for Medical Research, and the Alberta Cancer Board for supporting this project. Å. M. Ballangrud is a postdoctoral fellow supported by the Royal Norwegian Council of Industrial and Scientific Research.

REFERENCES

1. Wilson BC, Jacques SL. Optical reflectance and transmittance of tissues: Principles and applications. IEEE Journal of Quantum Electronics 1990; 26:2186–2199.
2. Wilson BC, Patterson MS, Flock ST. Indirect *versus* direct techniques for the measurement of the optical properties of tissues. Photochem Photobiol 1987; 46:601–608.
3. Arnfield MR, Mathew RP, Tulip J, McPhee MS. Analysis of tissue optical coefficients using an approximate equation valid for comparable absorption and scattering. Phys Med Biol 1992; 37:1219–1230.
4. Flock ST, Patterson MS, Wilson BC, Wyman DR. Monte Carlo modeling of light propagation in highly scattering tissues. I. Model predictions and comparison with diffusion theory. IEEE Transactions on biomedical engineering 1989; 36:1162–1168.
5. Patterson MS, Wilson BC, Wyman DR. The propagation of optical radiation in tissue. I. Models of radiation transport and their application. Lasers Med Sci 1991; 6:155–168.
6. Lilge L, Wilson BC. The accuracy of interstitial measurements of absolute light fluence rate in the determination of tissue optical properties. SPIE (Laser-Tissue Interaction IV) 1993; 1882:291–304.
7. Flock ST, Wilson BC, Patterson MS. Monte Carlo modeling of light propagation in highly scattering tissues. II. Comparison with measurements in phantoms. IEEE Trans Biomed Eng 1989; 36:1169–1173.
8. Star WM, Marijnissen JPA, van Gemert MJC. Light dosimetry in optical phantoms and tissues. I. Multiple flux and transport theory. Phys Med Biol 1988; 33:437–454.
9. Arnfield MR, Chapman JD, Tulip J, Fenning MC, McPhee MS. Optical properties of experimental prostate tumors *in vivo*. Photochem Photobiol 1993; 57:306–311.
10. Pantelides ML, Whitehurst C, Moore JV, King TA, Blacklock NJ. Photodynamic therapy for localised prostatic cancer: Light penetration in the human prostate gland. J Urol 1990; 143:398–401.
11. Whitehurst C, Pantelides ML, Moore JV, Brooman PJC, Blacklock NJ. *In vivo* laser light distribution in human prostatic carcinoma. J Urol 1994; 151:1411–1415.
12. Flock ST, Wilson BC, Patterson MS. Total attenuation coefficients and scattering phase functions of tissues and phantom materials at 633 nm. Med Phys 1987; 14:835–841.
13. Ballangrud ÅM, Wilson PJ, Miller GG, Moore RB, McPhee MS, Tulip J. Light distribution and optical coefficients in prostate tumor. SPIE 1994; 2371:148–152.
14. Cheong WF, Prahl SA, Welch AJ. A review of the optical properties of biological tissues. IEEE J Quant Electron 1990; 26:2166–2185.
15. Moes CJM, van Gemert MJC, Star WM, Marijnissen JPA, Prahl SA. Measurements and calculations of the energy fluence rate in a scattering and absorbing phantom at 633 nm. Applied Optics 1989; 28:2292–2296.
16. Grosjean CC. A high accuracy approximation for solving multiple scattering problems in infinite homogenous media. Nuovo Cimento 1956; 3:1263–1275.
17. Weinberg AM, Wigner EP. "The Physical Theory of Neutron Chain Reactors." Chicago Press, Chicago, 1958.
18. Flock ST, Jacques SL, Wilson BC, Star WM, van Gemert MJC. Optical properties of Intralipid: A phantom medium for light propagation studies. Lasers Surg Med 1992; 12:510–519.
19. van Staveren HJ, Moes CJM, van Marle J, Prahl SA, van Gemert MJC. Light scattering in Intralipid: 10% in the wavelength range of 400–1100 nm. Applied Optics 1991; 30:4507–4514.
20. Isaacs JT, Weissman RM, Coffey DS, Scott WW. Concepts in prostatic cancer biology: Dunning R3327-H, HI and AT tumors. Prog Clin Biol Res 1980; 37:311–323.
21. Lubaroff DM, Canfield L, Reynolds CW. The Dunning tumors. Prog Clin Biol Res 1980; 37:243–263.
22. Arnfield MR, Tulip J, McPhee MS. Photodynamic therapy dosimetry in postmortem and *in vivo* rat tumors and an optical phantom. Photochem Photobiol 1990; 51:667–674.